Evolution of bulk superconductivity in $SrFe_2As_2$ with Ni substitution

S. R. Saha, N. P. Butch, K. Kirshenbaum, and Johnpierre Paglione*
Center for Nanophysics and Advanced Materials, Department of Physics, University of Maryland, College Park, Maryland 20742, USA
(Received 6 May 2009; revised manuscript received 22 May 2009; published 16 June 2009)

Single crystals of the Ni-doped FeAs-based superconductor $SrFe_{2-x}Ni_xAs_2$ were grown using a self-flux solution method and characterized via x-ray measurements and low-temperature transport, magnetization, and specific heat studies. A doping phase diagram has been established where the antiferromagnetic order associated with the magnetostructural transition of the parent compound $SrFe_2As_2$ is gradually suppressed with increasing Ni concentration, giving way to bulk-phase superconductivity with a maximum transition temperature of 9.8 K. The superconducting phase exists through a finite range of Ni concentrations centered at $x=0.15$ with full diamagnetic screening observed over a narrow range of x coinciding with a sharpening of the superconducting transition and an absence of magnetic order. An enhancement of bulk superconducting transition temperatures of up to 20% was found to occur upon high-temperature annealing of samples.

DOI: 10.1103/PhysRevB.79.224519 PACS number(s): 74.25.Dw, 74.25.Fy, 74.25.Ha, 74.62.Dh

I. INTRODUCTION

The appearance of superconductivity in iron-based pnictide compounds has attracted much attention, providing both a new potential angle in understanding the physics of high-temperature superconductivity in other materials such as the copper oxides and an entire new family of superconducting materials of fundamental and technological interest. Superconductivity with $T_c=26$ K was first reported in $LaO_{1-x}F_xFeAs$ at ambient pressure[1] and later raised to 43 K under applied pressures.[2] The highest T_c achieved so far in these materials is about 55 K in $SmO_{1-x}F_xFeAs$ (Ref. 3) and (Ba,Sr,Ca)FeAsF (Refs. 4 and 5). Oxygen-free FeAs-based compounds with the $ThCr_2Si_2$-type (122) structure also exhibit superconductivity but so far at slightly lower temperatures with a maximum value of $T_c \simeq 37$ K induced by chemical substitution of alkali or transition-metal ions,[6–9] or by the application of large pressures.[10–13] A few stoichiometric FeAs-based 122 compounds including KFe_2As_2 and $CsFe_2As_2$ (Refs. 7 and 14) show superconductivity below 4 K at ambient pressures. Despite the lower values of T_c, the 122 compounds are an important experimental platform for understanding Fe-based superconductivity, as it is possible to synthesize large, high-quality single crystals whereas it is rather difficult for the 1111 compounds.

It is widely believed that suppression of the magnetic/structural phase transition in these materials, either by chemical doping or high pressure, is playing a key role in stabilizing superconductivity in the ferropnicitides.[15–17] For instance, superconductivity has been induced by partial substitution of Fe by other transition-metal elements like Co and Ni in both the 1111 (Refs. 18–20) and 122 compounds.[6,9] For the 122 phase, superconductivity with T_c as high as 25 K in $BaFe_{2-x}Co_xAs_2$ (Refs. 21 and 22) and $SrFe_{2-x}Co_xAs_2$ (Ref. 6) systems, and 21 K in $BaFe_{2-x}Ni_xAs_2$ (Refs. 17 and 23) has also been observed. Very recently, Ru, Ir, and Pd substitution for Fe was also shown to induce superconductivity in polycrystalline $SrFe_2As_2$ samples.[24–26] As implied by the enhanced negative thermoelectric power value in the normal state,[23,27] Co and Ni substitution appears to donate negative charge carriers that are thought to lead to superconductivity. Interestingly, in $BaFe_{2-x}Co_xAs_2$,[21,28] the maximum T_c is found at $x \simeq 0.17$ whereas in $BaFe_{2-x}Ni_xAs_2$, the maximum T_c occurs at approximately $x=0.10$ (Refs. 17 and 23), suggesting that Ni substitution may indeed contribute twice as many d electrons to the system as Co. Regarding this, an important question to ask is whether an analogous situation exists in a system with different structural parameters such as $SrFe_2As_2$. While there have been several studies[6,21,28] of $SrFe_{2-x}Co_xAs_2$, no bulk superconductivity has been reported in $SrFe_{2-x}Ni_xAs_2$.

To investigate the effects of Ni substitution in an as-yet unexplored series of the FeAs-based 122 compounds, a study of the evolution of superconductivity in single-crystalline $SrFe_{2-x}Ni_xAs_2$ was performed. Here we report superconductivity induced by Ni substitution in the series $SrFe_{2-x}Ni_xAs_2$ with maximum T_c (onset) of 9.8 K. By studying a wide range ($x=0-0.30$) of single-crystal samples, we establish a new member of the 122 series with superconductivity induced by transition-metal substitution for Fe. Contrary to expectations framed by prior studies of similar compounds, we observe a relatively low maximal T_c value of ~ 10 K in this series, centered at a Ni concentration approximately half that of the optimal Co concentration in $SrFe_{2-x}Co_xAs_2$.[21,28] Below, we discuss the evolution of electrical transport, magnetic and thermodynamic quantities as a function of Ni concentration, studying the characteristics of the doping-induced superconductivity in this system. We also discuss similarities and differences between this new superconducting system and other members of the 122 family of iron-pnictide superconductors.

II. EXPERIMENTAL

Single-crystalline samples of $SrFe_{2-x}Ni_xAs_2$ were grown using the FeAs self-flux method.[28] The FeAs and NiAs binary precursors were first synthesized by solid-state reaction of Fe (5N)/Ni (5N) powder with As (4N) powders in a quartz tube of partial atmospheric pressure of Ar. The precursor materials were mixed with elemental Sr (3N5) in the ratio $4-2x:2x:1$, placed in an alumina crucible and sealed in a quartz tube under partial Ar pressure. The mixture was heated to 1200 °C, slow cooled to a lower temperature and

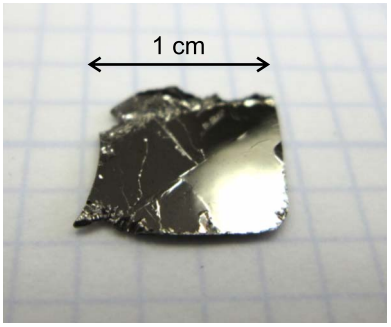

FIG. 1. (Color online) Digital image of a typical as-grown single crystal of $SrFe_{2-x}Ni_xAs_2$ harvested from flux growth. The arrow shows the large platelet dimension, indicative of crystals limited by crucible size.

then quenched to room temperature. Figure 1(a) presents a typical as-grown single-crystal specimen of $SrFe_{2-x}Ni_xAs_2$ with ~100 μm thickness and up to 1 cm width (the size of the crystals was typically found to be limited by the diameter of the crucibles).

Structural properties were characterized by both powder and single-crystal x-ray diffraction (XRD) and Rietfeld refinement (SHELXS-97) to $I4/mmm$ structure. XRD was performed at room temperature using a Siemens D5000 diffractometer with Cu-Kα radiation, with lattice parameters refined by a least-squares fit. Chemical analysis was obtained via wavelength-dispersive x-ray spectroscopy (WDS) and energy-dispersive x-ray spectroscopy (EDS), showing proper stoichiometry in all specimens reported herein and no indication of impurity phases.

Resistivity (ρ) samples were prepared using gold wire/silver paint contacts made at room temperature, yielding typical contact resistances of ~1 Ω. Resistance measurements were performed using the standard four-probe ac method, with excitation currents of 1 mA at higher temperatures that were reduced to 0.3 mA at low temperatures to avoid self-heating, all driven at 17 Hz frequency. Magnetic susceptibility (χ) was measured using a Quantum Design superconducting quantum interference device (SQUID) magnetometer and specific heat was measured with a Quantum Design cryostat using the thermal relaxation method.

III. RESULTS AND DISCUSSION

A. Structural and chemical characterization

Figure 2(a) presents crystallographic a- and c-axis lattice constants determined from refinement fits of x-ray diffraction patterns of powdered samples of $SrFe_{2-x}Ni_xAs_2$ as a function of Ni concentration x, along with the resultant tetragonal ratio c/a shown in Fig. 2(b). With increasing x, the c-axis lattice constant decreases and the a-axis lattice constant increases while the c/a ratio decreases linearly without any significant change in unit-cell volume to within experimental accuracy. Figure 2(c) shows the actual Ni-concentration determination in $SrFe_{2-x}Ni_xAs_2$ crystals measured by WDS analysis, using an average value determined from ten different spots on each specimen, plotted as a function of nominal

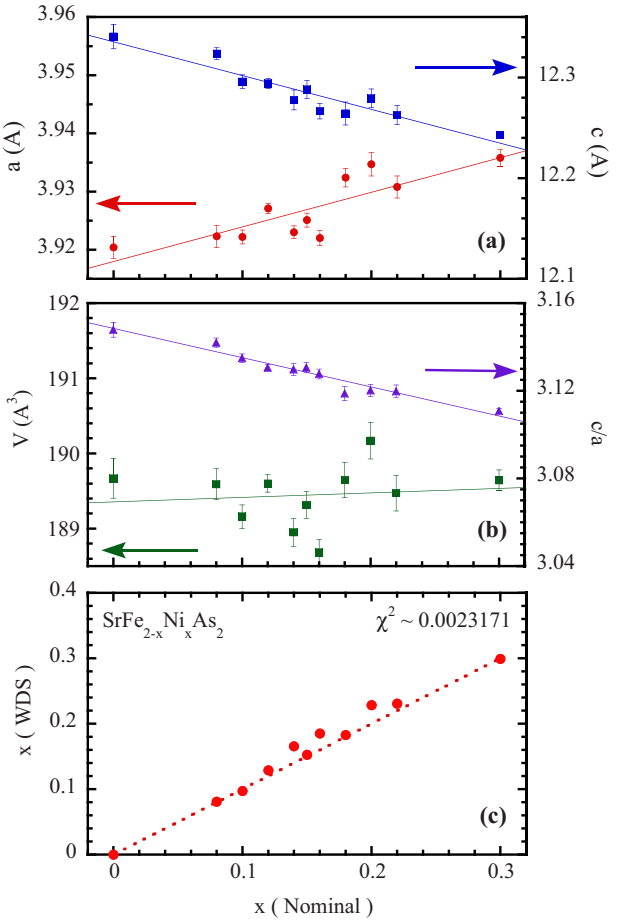

FIG. 2. (Color online) (a) Variation in the a- and c-axis lattice constants of $SrFe_{2-x}Ni_xAs_2$ with Ni content x, as determined from Rietfeld refinement of x-ray powder-diffraction spectra; (b) corresponding change in tetragonal c/a ratio and unit-cell volume V; (c) actual Ni concentration of $SrFe_{2-x}Ni_xAs_2$ single-crystal samples as a function of nominal concentration x, as determined by wavelength-dispersive x-ray spectroscopy (data points represent average value of ten scanned points for each concentration, the dotted line is a linear fit with a slope of 1).

concentration x. Because a linear fit (dotted line) results in a slope of unity to within scatter, the nominal value of x will be used hereafter as an adequate representation of the actual concentration.

B. Electrical resistivity

Figure 3(a) presents the comparison of the in-plane resistivity $\rho(T)$ of single crystals of $SrFe_{2-x}Ni_xAs_2$ (data are presented after normalizing to room temperature and offsetting for clarity). As shown, $\rho(T)$ data for $SrFe_2As_2$ exhibit metallic behavior, decreasing with temperature from 300 K before exhibiting a sharp kink at T_0=198 K, where a structural phase transition (from tetragonal to orthorhombic upon cooling) is known to coincide with the onset of antiferromagnetic (AFM) order.[29] With increasing Ni substitution the anomaly associated with T_0 becomes less distinct and is defined by a smooth minimum in $\rho(T)$, which shifts to lower temperature as indicated by the position of short arrows in Fig. 3(a),

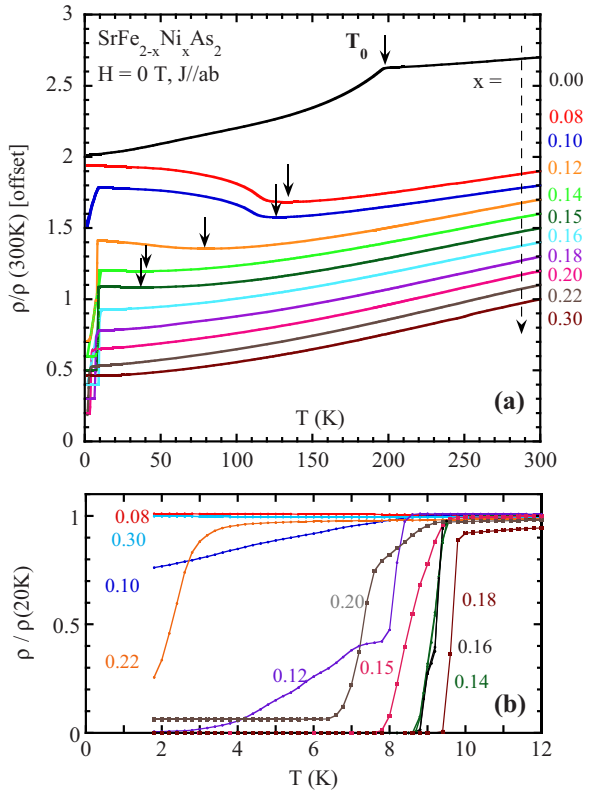

FIG. 3. (Color online) (a) Temperature dependence of in-plane electrical resistivity of specimens of $SrFe_{2-x}Ni_xAs_2$, normalized to 300 K and offset for clarity (data sets placed above $x=0.30$ are successively offset vertically by 0.1, except for $x=0$ data, which are offset by 1.7). The direction of the broken arrow indicates the order of the resistivity curves with ascending x as noted to the right. Short arrows indicate the position of the magnetic transition T_0, defined by the kink in $x=0$ data and the minima in $\rho(T)$ data for $0.08 \leq x \leq 0.15$. (b) Expanded low-temperature view of resistivity normalized to 20 K for clarity showing the evolution of superconducting transitions with Ni concentration.

finally disappearing for $x>0.15$, where no minimum is evident. We define the value of T_0 as the position of the kink in $x=0$ data and the position of the minima in $\rho(T)$ data for $0.08 \leq x \leq 0.15$ and present its evolution with Ni concentration in Fig. 4.

The sharp decrease in $\rho(T)$ associated with T_0 in the undoped material is observed to change character with increased Ni substitution, as it is shifted to lower temperatures. This switch, from a drop in $\rho(T)$ to a rise in $\rho(T)$ with decreasing T as T_0 is suppressed, has also been observed in other doped 122 materials,[6,17,22,23] and likely arises due to a shift in the balance between the loss of inelastic scattering due to the onset of magnetic order and the change in carrier concentration associated with the transition at T_0. Interestingly, the substitution of Ni for Fe appears to have minimal effect on inelastic scattering in the paramagnetic state, as indicated by the identical slope and curvature of all $\rho(T)$ curves above T_0 in Fig. 3(a). This can be considered as a confirmation of the dominant role of phonon scattering in determining the temperature dependence of resistivity.

For $x=0$, ρ continues to decrease below T_0 without any trace of superconductivity down to 1.8 K. (The appearance

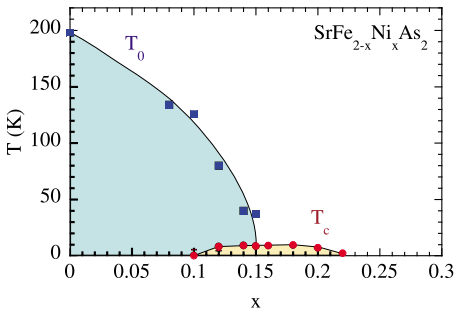

FIG. 4. (Color online) Ni-substitution phase diagram of $SrFe_{2-x}Ni_xAs_2$ obtained from electrical resistivity data, showing the suppression of the magnetic/structural phase transition T_0 (blue squares) with increasing Ni concentration, and the appearance of a superconducting transition (red circles) with maximum T_c of ~ 10 K centered around $x \simeq 0.15$.

of strain-induced superconductivity with $T_c=21$ K has been previously shown to appear in undoped ($x=0$) samples of $SrFe_2As_2$.[30] However here we present $x=0$ data for a sample with all traces of superconductivity removed by heat treatment.) This is also the case for $x=0.08$, with no evidence of superconductivity down to 1.8 K. However, $x=0.1$ begins to show traces of superconductivity as evidenced by a partial drop in $\rho(T)$ below ~ 10 K as shown in Fig. 3(b). For $x=0.12$, there is a sharp drop below 8.4 K that does reach zero resistance at lower temperatures. This partial transition turns into a full transition for $x \geq 0.14$ with higher T_c. In the range of samples studied, the highest T_c is obtained for $x=0.18$ with a ~ 9.8 K onset and ~ 9.6 K midpoint. For $x \geq 0.2$, superconductivity becomes partial again with incomplete superconducting transitions shown in the $x=0.20$ and $x=0.22$ samples and the complete absence of any superconducting transition down to 1.8 K for $x=0.3$.

Figure 4 presents the phase diagram representing the variation in T_0 and T_c (determined as noted above and at the 50% drop of ρ, respectively), as a function of Ni content x. The superconducting window spans the range $x=0.1-0.22$ [see also Fig. 7(d) below for a detailed view] and forms a domelike superconducting phase that appears qualitatively similar to other Co- and Ni-doped 122 compounds.

C. Magnetic susceptibility

Figure 5(a) presents the temperature dependence of magnetic susceptibility χ of $SrFe_{2-x}Ni_xAs_2$ crystals, measured under zero-field-cooled (ZFC) conditions by applying 10 mT along the ab plane. The data are presented with a y-axis offset for clarity purposes ($x=0$ data have been shifted by $+0.0015$ cm^3/mol and successive data sets for $x>0$ have been staggered downward), however note that absolute values at room temperature for all Ni concentrations are all approximately $\chi(300\ \mathrm{K}) \simeq 0.001$ cm^3/mol to within experimental error. As shown, the overall behavior of low-field susceptibility for $x=0$ is similar to that reported previously[29] for high-field conditions, showing a modest temperature dependence interrupted by a sharp drop at T_0 due to the magnetic/structural transition. The overall temperature dependence and magnitude of χ remains more or less constant

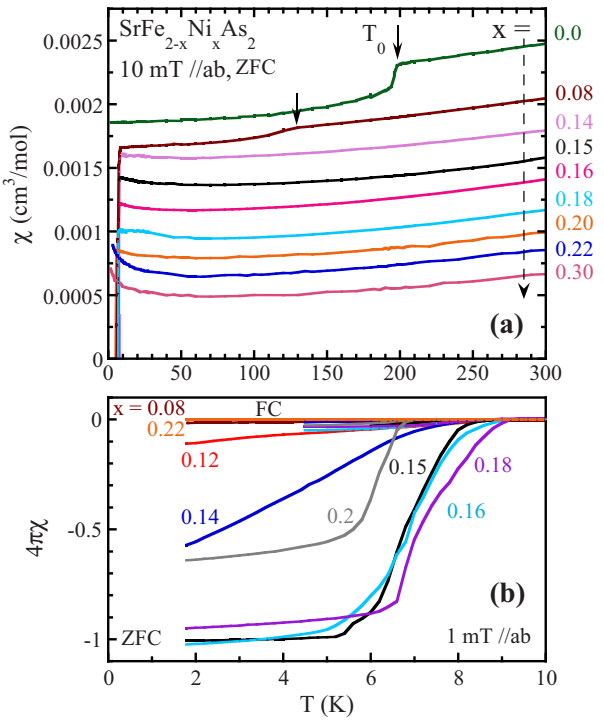

FIG. 5. (Color online) Temperature dependence of magnetic susceptibility χ of $SrFe_{2-x}Ni_xAs_2$, measured with 10 mT field applied parallel to the crystallographic basal plane from ZFC conditions, offset for clarity ($x=0$ data are vertically offset by +0.0015 cm^3/mol with other sets offset successively downward by ~0.0002). (b) Low-temperature zoom of the volume magnetic susceptibility in $SrFe_{2-x}Ni_xAs_2$ crystals under 1 mT ZFC and FC conditions after a 24 h/700 °C annealing treatment (see text for details).

with Ni doping, indicating minimal impact of Ni substitution on the paramagnetic susceptibility of $SrFe_{2-x}Ni_xAs_2$. With increasing Ni concentration, the large steplike feature at T_0 is suppressed to lower temperatures and dramatically reduced in magnitude, as indicated by a small kink at T_0 for $x=0.08$ and no discernible feature for higher x. This behavior is comparable to the effect of Co doping in the $BaFe_{2-x}Co_xAs_2$ series,[22] which shows a similar trend in magnetization data taken at 1 T.

Note that the low-field $\chi(T)$ data presented here do not show any significant increase at low temperatures, indicating both good sample quality (i.e., minimal magnetic impurity content) and no indication of strain-induced superconductivity.[30] A very small upturn in $\chi(T)$ does appear to onset at low temperatures in all Ni-doped samples. Although its magnitude is quite small, the systematic presence of this upturn along with its slight enhancement in higher Ni-doped samples (i.e., $x=0.22$ and 0.30 data sets) suggests the presence of either a small magnetic impurity content or a small local-moment contribution, possibly due to the presence of Ni. Because a Curie-type tail was reported in $SrFe_2As_2$ samples even at high (5 T) fields, albeit with a much more pronounced increase at low temperatures,[29] impurity contributions are less likely. In any case, more work is required to discern the origin of this feature.

Shown in Fig. 5(b) are the low-temperature susceptibility data for $SrFe_{2-x}Ni_xAs_2$ samples measured with a smaller applied field of 1 mT along the *ab* plane under both ZFC and field-cooled (FC) conditions, plotted as the volume susceptibility $4\pi\chi$ to compare the level of diamagnetic screening due to superconductivity. As shown, the superconducting volume fraction, as estimated by the fraction of full diamagnetic screening ($4\pi\chi=-1$), varies with Ni concentration, being absent for $x<0.12$, partial for $x=0.12$, 0.14, and 0.20, and complete for $x=0.15$, 16, and 0.18. This suggests that there is indeed a full superconducting volume fraction observed for a range of Ni concentrations with maximized T_c values but also that partial-volume fractions are evident at the fringes of the superconducting dome. For instance, note that a drop in $\chi(T)$ is visible below 7 K in the $x=0.08$ data shown in Fig. 5(a) but also that the volume fraction associated with this diamagnetic screening is very small, being less than ~1% as evident from Fig. 5(b). Likewise, data for $x=0.12$ show a somewhat larger response but still remain at much less than 100%. This is quantified in Fig. 7 in comparison to other quantities of interest, as discussed below.

D. Specific heat

To verify the bulk thermodynamic nature of the superconducting transition in $SrFe_{2-x}Ni_xAs_2$, we performed specific heat measurements on an annealed sample with optimal Ni concentration of $x=0.15$. The electronic specific heat C_e was determined by subtracting the phonon contribution from the total specific heat at zero magnetic field. Fitting of the $x=0.15$ data to the standard form $C_p=\gamma T+\beta T^3$ for the total specific heat through the range $75\leq T^2\leq 290$ K^2 yields an electronic contribution $\gamma=32$ $mJ/mol\,K^2$ and a phononic contribution $\beta=0.76$ $mJ/mol\,K^4$, the latter value corresponding to a Debye temperature of $\Theta_D=234$ K. For $x=0$ (not shown), C_e/T is almost independent of T at low temperatures down to 2 K to within the experimental accuracy, exhibiting comparable fit parameters to those above and thus verifying that no significant change in the phonon spectrum is imparted by Ni substitution.

Figure 6 presents the low-temperature portion of C_e/T for $x=0.15$, highlighting the onset of a weak anomaly below 8.5 K that is consistent with the value of T_c deduced from $\chi(T)$ measurements. Although the peak in C_e/T is too poorly defined to fit with an equal entropy construction, a rough quantitative characterization provides an estimated value of $\Delta C/\gamma T_c\simeq 0.12$. This is much smaller than the BCS expectation of 1.52 for a superconducting transition but is not surprising considering the similar trend found in the literature. Although a sizeable specific heat anomaly has been observed at the superconducting transition of some Fe-based superconductors, including values near the BCS expectation in both $Ba_{0.6}K_{0.4}Fe_2As_2$ (Ref. 31) and LaFePO (Ref. 32), it is intriguing that many members of the FeAs-based family—including both Co-doped $BaFe_2As_2$ (Ref. 21) and $CaFe_2As_2$ (Ref. 33), and F-doped LaFeAsO (Ref. 34) and SmFeAsO (Ref. 35)—exhibit rather weak signatures of superconductivity in specific heat measurements, despite indications of bulk diamagnetic screening from magnetization measurements.

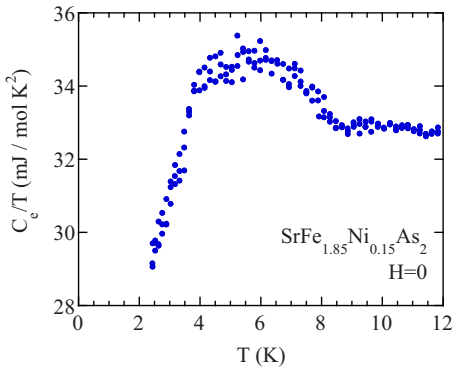

FIG. 6. (Color online) Temperature dependence of the electronic specific heat C_e in $SrFe_{1.85}Ni_{0.15}As_2$ obtained by standard fitting and subtraction of a phonon contribution to the total specific heat (see text). Data show a small but distinct transition consistent with superconductivity below T_c=8.5 K determined from magnetic-susceptibility measurements.

Likewise, the anomaly in the specific heat of the x=0.15 sample of $SrFe_{2-x}Ni_xAs_2$ shown in Fig. 6 is surprisingly small. The small peak observed in several of these materials would normally seem to reflect a need to improve sample quality via improved growth techniques or annealing treatment, as was indeed shown for the case of LaFePO.[32] However, measurements of C_e/T in an as-grown unannealed x =0.15 sample of $SrFe_{2-x}Ni_xAs_2$ (not shown) also present a weak feature at T_c quantitatively comparable in magnitude to that discussed above for the annealed sample. In light of the enhancement of T_c invoked by annealing discussed below, this suggests that, at least for the case of $SrFe_{2-x}Ni_xAs_2$, improvements in the superconducting properties do not lead to enhanced values of $\Delta C/\gamma T_c$ as would be expected for improved sample quality. More important, the small values of $\Delta C/\gamma T_c$ observed in many FeAs-based materials are difficult to reconcile with consistent observations of bulk diamagnetic screening, including those for many $SrFe_{2-x}Ni_xAs_2$ samples in this study of widely varying size and shape. Overall, this suggests that a lack of sample quality may not always be responsible for poor thermodynamic signatures of superconductivity in these materials and that alternative explanations should not yet be ruled out. For instance, the small size of $\Delta C/\gamma T_c$ in $SrFe_{2-x}Ni_xAs_2$ and the large residual density of states may imply that superconductivity gaps only a small part of the Fermi surface.

E. Doping evolution

It is instructive to compare the evolution of the superconducting state parameters in more detail as a function of Ni concentration. In Fig. 7, we compare measures of the width of the superconducting transition ΔT_c as defined by the difference of T_c at 90% and 10% drop of resistivity from its normal-state value, the estimated superconducting volume fraction determined from the level of diamagnetic screening and the evolution of T_c itself as determined by transitions in both resistivity and susceptibility. These parameters are plotted alongside the values of residual resistivity $\rho_0(x)$ (determined by linear extrapolations from above T_c) to compare

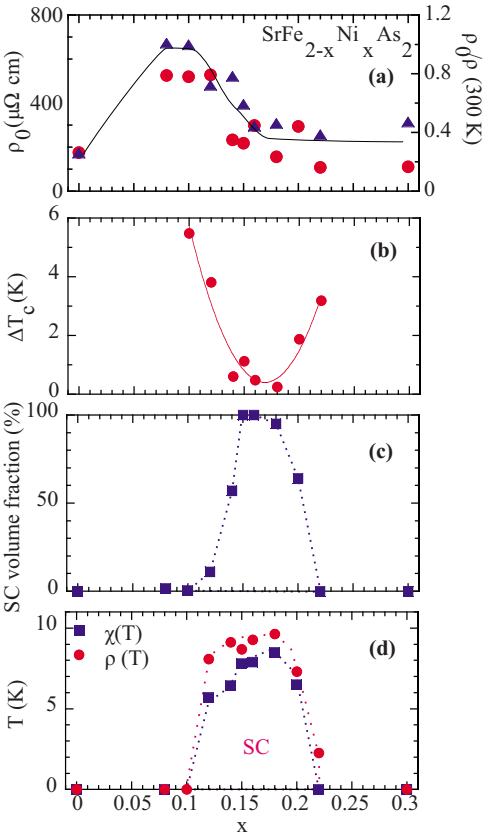

FIG. 7. (Color online) Evolution of normal and superconducting state parameters in $SrFe_{2-x}Ni_xAs_2$ with Ni concentration x: (a) absolute (circles—left scale) and normalized (triangles—right scale) residual resistivity; (b) variation in the width in temperature of the resistive superconducting transition ΔT_c; (c) superconducting volume fraction determined from the magnetic susceptibility data; (d) expanded view of the superconducting phase determined by transition temperatures defined by 50% resistivity drop (circles) and 10% value of total diamagnetic screening (blue squares). All lines are guides.

the evolution of superconductivity with residual transport scattering behavior, also used as a measure of where magnetic order is suppressed.

The evolution of ρ_0 with Ni doping is plotted in Fig. 7(a), including both the absolute value of ρ_0 (left y axis) and that normalized by ρ(300 K) (right y axis) to remove uncertainty in geometric factors. As a function of x, both absolute and normalized values of $\rho_0(x)$ follow a similar pattern, suggesting that geometric factor errors are not large. As shown in Fig. 7(a), an increase in resistivity occurs with increasing Ni concentration between x=0 and 0.08 before showing an approximate plateau up to x=0.12, reflecting the change in transport scattering associated with magnetic order at low concentrations. Above x=0.12, ρ_0 shows a rapid decrease with increasing x before again leveling off at higher Ni concentration, coincident with the complete suppression of magnetic order near x=0.15 and the onset of superconductivity. This trend follows what can be inferred from the $\rho(T)$ data found in Fig. 3(a), with an enhancement of ρ_0 found only in the regime $(0<x<0.12)$, where inelastic scattering is greatly enhanced by the presence of magnetic order, resulting in an increase in $\rho(T)$ below T_0.

Interestingly, aside from this enhancement, the impurity scattering level [as measured by the value of $\rho_0(x)$] does not show any significant change with Ni concentration, with values of ρ_0 in high Ni-content samples approaching that of $\rho(x=0)$. In a minimal model where residual resistivity is dominated by impurity/disorder scattering, this trend would suggest that Ni substitution for Fe introduces minimal disorder into the system, even up to $x=0.30$ levels. However, it is likely that a more unconventional mechanism (such as magnetic fluctuation scattering) may dominate the value of ρ_0 in this system, thereby masking the underlying (small) increase in residual scattering due to Fe site disorder.

A detailed plot of T_c vs x is presented in Fig. 7(d), showing good agreement between T_c values determined by transitions in $\rho(T)$ and $\chi(T)$. As is evident from the comparison of $\rho_0(x)$ to $T_c(x)$ in Fig. 7, the rather abrupt decrease in residual scattering occurs very close to the appearance of bulk superconductivity in $SrFe_{2-x}Ni_xAs_2$. The Ni concentration of $x=0.14$ is where ρ_0 drops to its low value and a sizeable volume fraction of superconductivity first appears, as shown in Fig. 7(b). Both the width ΔT_c of the transition and the superconducting volume fraction change dramatically in this concentration range. As shown, there is an interesting inverse correlation between ΔT_c and this volume fraction within the range of superconducting samples, illustrating that the sharpest superconducting transitions are associated with bulk superconductivity while the broader transitions are associated with only partial-volume superconductivity.

With the current set of measurements, it is hard to distinguish whether there is an inhomogeneous distribution of Ni content in the samples close to this boundary causing the partial superconducting transitions or whether the narrow range of bulk superconductivity is truly an intrinsic property. However, several factors suggest that inhomogeneity in Ni concentration should not be significant. First, x-ray diffraction and chemical analysis data presented in Fig. 2 suggest that Ni substitution is occurring smoothly and continuously in this series with no observable deviations at the edges of the superconducting dome. Second, both resistivity and susceptibility data presented above also progress smoothly as a function of x, again indicating no major levels of phase separation. Finally, note that all $SrFe_{2-x}Ni_xAs_2$ crystalline samples used in this study have been annealed at high temperatures to further reduce smaller inhomogeneity levels, as discussed below.

F. Annealing effect on superconductivity

One method of investigating the effect of crystalline quality is by high-temperature heat treatment. Interestingly, we found that annealing single crystals of $SrFe_{2-x}Ni_xAs_2$ in such a way produces a rather dramatic enhancement in the value of T_c. Specifically, holding samples at 700 °C for 24 h in an Ar atmosphere was found to increase T_c by up to ~1 K. As shown in Fig. 8, the effect of annealing on the superconducting transition in $SrFe_{1.85}Ni_{0.15}As_2$ crystals is evident in both $\rho(T)$ and $\chi(T)$, indicating that this enhancement is reflected in the full diamagnetic screening and is therefore a bulk phenomenon. Such an enhancement of T_c could be an indication

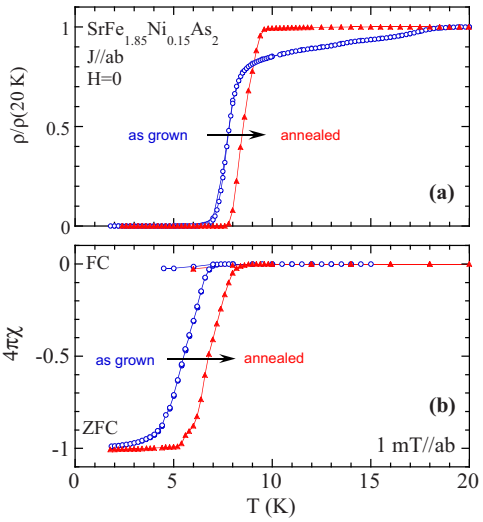

FIG. 8. (Color online) Effect of high-temperature annealing on an optimally doped $x=0.15$ sample of $SrFe_{2-x}Ni_xAs_2$, demonstrating typical results from before and after a 24 h, 700 °C heat treatment performed on a sample sealed in a quartz tube with a pure argon environment. (a) Resistivity data of a $x=0.15$ sample measured before (blue circles) and after (red triangles) heat treatment. (b) Volume magnetic susceptibility of a $x=0.15$ sample at low fields measured before (blue circles) and after (red triangles) annealing. Arrows emphasize enhancement of T_c by annealing, with good agreement in T_c values for both cases.

of improved crystallinity due to release of residual strain and/or improved microscopic chemical homogeneity of Ni content inside the specimens, thereby optimizing the stability of superconductivity. A similar annealing effect was reported in LnFeOP (Ln=La, Pr, and Nd) single crystals, where a heat treatment in flowing oxygen was also found to improve superconducting properties.[32]

It is further noteworthy to report that as-grown crystals of $SrFe_{2-x}Ni_xAs_2$ for $x<0.16$ show what looks to be a partial superconducting transition near 20 K that is completely removed by heat treatment, as demonstrated in Fig. 8(a) for $x=0.15$. Although it is tempting to posit that 20 K is a possible value for optimal T_c in this series of Ni-substituted compounds, note that aside from the enhancement of T_c as mentioned above, the removal of this feature is the only change observed in measured quantities imposed by annealing: neither the resistivity nor the magnetic susceptibility in the normal state show any change after annealing. Furthermore, susceptibility does not show any indication of diamagnetic screening above bulk T_c values in the as-grown samples. Because the 20 K kink is removed with heat treatment, and moreover, is always found to be positioned near the same temperature, we believe this feature may be connected to the strain-induced superconductivity found in undoped $SrFe_2As_2$.[30] However, note that whereas only a mild 5 min heat treatment of 300 °C removes the partial-volume superconductivity in $SrFe_2As_2$, a substantially higher-temperature 700 °C treatment is required to remove this feature in $SrFe_{2-x}Ni_xAs_2$. If the two phenomena are related, it is possible that internal strain is stabilized by the chemical inhomogeneity associated with transition-metal substitution in

$SrFe_{2-x}Ni_xAs_2$ thus requiring higher temperatures to be removed. More systematic studies of the effect of annealing on $SrFe_{2-x}Ni_xAs_2$ are under way to investigate this relationship.

G. Comparison to other FeAs-based systems

Superconductivity appears in $SrFe_{2-x}Ni_xAs_2$ through the range $x=0.1-0.22$, tracing out a domelike T_c curve qualitatively similar to other transition-metal-substituted FeAs-based superconducting systems. Naively, in a rigid-band model it would be expected that each Ni^{2+} dopant introduces two extra itinerant $3d$ electrons while each Co^{2+} dopant adds only one. In $SrFe_{2-x}Ni_xAs_2$, the superconducting phase is centered about an "optimal" Ni concentration of $x\simeq 0.15$ that corresponds to 7.5% Ni substitution for Fe, which is indeed approximately half of the median concentration of Co ($\sim 0.25-0.30$) which induces superconductivity in $SrFe_{2-x}Co_xAs_2$ through the range $0.15<x<0.40$.[6] This is comparable to the case of $BaFe_{2-x}Ni_xAs_2$ and $BaFe_{2-x}Co_xAs_2$, where the superconducting phases are centered on $x\simeq 0.10$ and $x\simeq 0.17$, respectively,[17,21,23] also roughly following the d-electron counting trend. What is intriguing, however, is that the absolute percentage of Fe substitution required to induce superconductivity in Sr- and Ba-based 122 systems by the same dopant atom appears to be different. In $SrFe_{2-x}Ni_xAs_2$, the optimal Ni concentration of $\sim 7.5\%$ is at least ~ 1.5 times the optimal Ni concentration in both $BaFe_{2-x}Ni_xAs_2$, where $x\simeq 0.10$ corresponds to 5% Fe substitution,[17,23] and the related 1111 compound $LaFe_{1-x}Ni_xAsO$, where $x\simeq 0.04$ corresponds to 4% Fe substitution.[20]

Interestingly, the *onset* of superconductivity in Co- and Ni-doped $SrFe_2As_2$ appears to occur near the same substitution concentration of $x\simeq 0.1$ but with T_c much suppressed in the $SrFe_{2-x}Ni_xAs_2$ system relative to that of $SrFe_{2-x}Co_xAs_2$. This trend also appears to hold to some degree in the doped $BaFe_2As_2$ system, where the onset concentration for $BaFe_{2-x}Ni_xAs_2$ is approximately the same as that of $BaFe_{2-x}Co_xAs_2$ while its maximum T_c value is somewhat reduced.[17] However the comparison between Ba- and Sr-based 122 materials may not be so straightforward owing to the different alkali earth ions involved. Instead, it is simpler to directly compare the effect of substituting different $3d$ and $4d$ metal substitutions in the same Sr-based parent material $SrFe_2As_2$. Shown in Fig. 9 is a comparison of the evolution of the superconducting phase in $SrFe_{2-x}Ni_xAs_2$ as compared to that of three other characteristic substitution series: Co doping,[6] Rh doping,[36] and Pd doping,[26] providing a complete comparison of the effects of d-electron doping with $3d$ vs $4d$ electrons. Notably, the trend noted above is strikingly similar in the Rh/Pd comparison, which also point to the same onset concentration of $x\simeq 0.1$ and a maximum T_c in the Pd-doped system that is also greatly reduced as compared to the Rh-doped system, reaching only ~ 9 K (Ref. 26) as compared to ~ 22 K (Ref. 36).

The comparable trends in these two sets of systems raise questions as to the nature of (1) the similar onset concentration in all compounds and (2) the inhibited T_c values in the two-electron-doped systems (i.e., Ni and Pd) as compared to the one-electron-doped systems (i.e., Co and Rh). One possible explanation lies in the differences in structural parameters as a function of doping. In $SrFe_{2-x}Ni_xAs_2$, the lattice constants increase along a axis and decrease along the c axis as a function of x, similar to the behavior for substituting Co, Pd, and Ru in $SrFe_2As_2$.[6,26,36] Also, the variation in c/a ratio with x in $SrFe_{2-x}Ni_xAs_2$ is close to that in $SrFe_{2-x}Co_xAs_2$,[6] although the maximum value of T_c is higher in the latter. On the other hand, the variation in c/a ratio with x in $SrFe_{2-x}Ni_xAs_2$ is different from that found in $SrFe_{2-x}Pd_xAs_2$,[26] while the maximum value of T_c is similar in these nominally isoelectronic systems. In other words, there is no obvious correlation between T_c and c/a ratio, at least in the $SrFe_2As_2$ derived superconductors, that could explain these phenomena. However, note that the shape of the distorted tetrahedral environment of Fe, likely an important structural parameter, may not have such a simple correlation with lattice parameters and may depend on how the As z coordinate changes with doping.

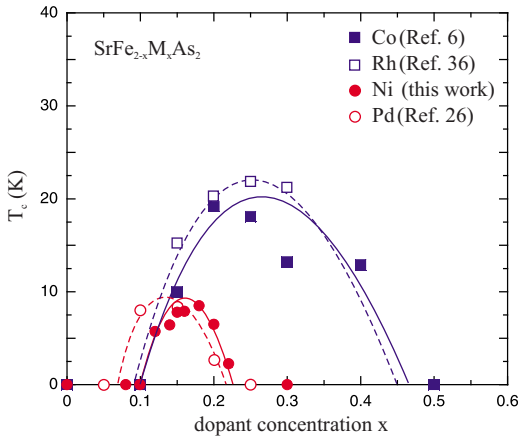

FIG. 9. (Color online) Comparison of the evolution of superconductivity as a function of Ni substitution in $SrFe_{2-x}Ni_xAs_2$ as compared to that previously observed in other transition-metal substitution series, with M=Co, Rh, and Pd (Refs. 6, 36, and 26, respectively). Solid symbols denote T_c values for $3d$-electron substituents Co (blue square) and Ni (red circle), and open symbols denote those of $4d$ substituents Rh (blue square) and Pd (red circle).

It is also important to consider the role of magnetism in stabilizing superconductivity in the FeAs-based materials. The related and widely perceived picture is that doping electrons or holes into the parent phase gradually suppresses magnetic order with pairing arising through the interpocket scattering of electrons via exchange of AF spin fluctuations.[37–40] Alternatively, magnetic order and superconductivity may compete to gap similar parts of the Fermi surface with superconductivity only appearing when magnetic order is suppressed. Either way, there is no doubt that superconductivity is strongly coupled, directly or indirectly, to the suppression of magnetic order in the FeAs-based 122 systems. As presented previously in Fig. 4, superconductivity in $SrFe_{2-x}Ni_xAs_2$ indeed appears through a range of Ni concentrations close to where magnetism is suppressed, similar to several other systems.[6,9,17,21,22,24–26] In $SrFe_{2-x}Ni_xAs_2$, the critical concentration appears to sit close to the optimal-doping concentration of $x\simeq 0.15$; it is of obvious interest to

determine this value to a more precise degree, along with that for the other transition-metal-substituted series as discussed above. This will require better methods of determining the magnetic transition temperature T_0, as is possible via neutron scattering experiments.

Interestingly, recent evidence of coexistent magnetic and superconducting phases on the "underdoped" side of the T_c dome in $BaFe_{2-x}Co_xAs_2$ point to a competitive coexistence of these phases.[41] The onset of T_c in $SrFe_{2-x}Ni_xAs_2$ appears to be rather abrupt, at least more so than the smooth onset observed in $BaFe_{2-x}Co_xAs_2$.[21,22] This may be due to a number of factors or differences between these systems, however it is tempting to posit that superconductivity and magnetism are more antagonistic in this system than in its Co-doped counterpart. In any case, it will be important to compare and contrast the detailed nature of these phase diagrams in order to gain a better understanding of nature of the interplay of magnetism and superconductivity.

Finally, it is interesting to note that superconductivity appears to occur over much narrower doping ranges in both Ni- and Pd-substituted 122 systems with lower maximum T_c values in Ni (Pd)-substituted materials as compared to Co (Rh) substitution. Together, these contrasts may indicate that the doping ranges that induce superconductivity may not only be simply shifted by effective *d*-electron doping level but may also involve an inherent suppression of T_c that increases with deviations from the presumably ideal Fe *d*-shell configuration, possibly due to details of a chemical nature. Such a picture is indeed consistent with the recent study of Cu doping in $BaFe_2As_2$,[17] where Cu is assumed to supply three additional *d* electrons and thereby deviate strongly from the Fe *d*-shell configuration. Conversely, studies of Ru-doped $SrFe_2As_2$,[24] involving nominally isovalent Fe substitution, support the scenario where superconductivity is most favored by transition-metal substitutions that minimally disrupt the Fe electronic environment. Of course, one must note that superconductivity is also known to be present in the fully Ni-substituted end-member $SrNi_2As_2$ (a low-temperature superconductor with $T_c=0.7$ K),[42] although its relationship to the superconductivity in $SrFe_{2-x}Ni_xAs_2$ is unclear. In any case, this puzzling point certainly warrants further investigation, for instance via careful inspections of the phase diagrams arising in single crystals using other transition-metal substituents, and the role of crystalline quality and disorder in suppressing superconductivity.

IV. SUMMARY

In summary, single crystals of the Ni-substituted series $SrFe_{2-x}Ni_xAs_2$ were successfully synthesized, allowing a determination of the phase diagram across which magneto-structural order is suppressed and superconductivity arises over a finite window. Upon suppression of magnetism, a phase of bulk superconductivity centered near an optimal concentration of $x \simeq 0.15$ is established with T_c values reaching as high as ~ 9.8 K. Interestingly, annealing treatments of as-grown crystals result in a significant enhancement of up to 20% in superconducting transition temperatures across this range. In comparison to its Co-doped counterpart, the observed superconducting phase in Ni-doped $SrFe_{2-x}Ni_xAs_2$ is intriguingly narrow and strongly suppressed but it shows similarities to other transition-metal-doped systems undergoing equivalent *d*-electron substitution, suggesting that similar underlying physics is at play in stabilizing superconductivity in several FeAs-based materials.

ACKNOWLEDGMENTS

The authors acknowledge P. Y. Zavalij and B. W. Eichhorn for experimental assistance and P. Bach, K. Jin, X. Zhang, and R. L. Greene for useful discussions. N.P.B. acknowledges support from CNAM.

*paglione@umd.edu

[1] Y. Kamihara, T. Watanabe, M. Hirano, and H. Hosono, J. Am. Chem. Soc. **130**, 3296 (2008).
[2] H. Takahashi, K. Igawa, K. Arii, Y. Kamihara, M. Hirano, and H. Hosono, Nature (London) **453**, 376 (2008).
[3] Z.-A. Ren, W. Lu, J. Yang, W. Yi, X.-L. Shen, Zheng-Cai, G.-C. Che, X.-L. Dong, L.-L. Sun, F. Zhou, and Z.-X. Zhao, Chin. Phys. Lett. **25**, 2215 (2008).
[4] X. Zhu, F. Han, P. Cheng, G. Mu, B. Shen, and H. H. Wen, Europhys. Lett. **85**, 17011 (2009).
[5] P. Cheng, B. Shen, G. Mu, X. Zhu, F. Han, B. Zeng, and H. H. Wen, Europhys. Lett. **85**, 67003 (2009).
[6] A. Leithe-Jasper, W. Schnelle, C. Geibel, and H. Rosner, Phys. Rev. Lett. **101**, 207004 (2008).
[7] K. Sasmal, B. Lv, B. Lorenz, A. M. Guloy, F. Chen, Y.-Y. Xue, and C.-W. Chu, Phys. Rev. Lett. **101**, 107007 (2008).
[8] M. Rotter, M. Tegel, and D. Johrendt, Phys. Rev. Lett. **101**, 107006 (2008).
[9] A. S. Sefat, R. Jin, M. A. McGuire, B. C. Sales, D. J. Singh, and D. Mandrus, Phys. Rev. Lett. **101**, 117004 (2008).
[10] M. S. Torikachvili S. L. Bud'ko N. Ni, and P. C. Canfield, Phys. Rev. Lett. **101**, 057006 (2008).
[11] T. Park, E. Park, H. Lee, T. Klimczuk, E. D. Bauer, F. Ronning, and J. D. Thompson, J. Phys.: Condens. Matt. **20**, 322204 (2008).
[12] P. L. Alireza, Y. T. Chris-Ko, J. Gillett, C. M. Petrone, J. M. Cole, G. G. Lonzarich, and S. E. Sebastian, J. Phys.: Condens. Matt. **21**, 012208 (2009).
[13] M. Kumar, M. Nicklas, A. Jesche, N. Caroca-Canales, M. Schmitt, M. Hanfland, D. Kasinathan, U. Schwarz, H. Rosner, and C. Geibel, Phys. Rev. B **78**, 184516 (2008).
[14] M. Rotter, M. Pangerl, M. Tegel, and D. Johrendt, Angew. Chem. **47**, 7949 (2008).
[15] C.-H. Lee, A. Iyo, H. Eisaki, H. Kito, M. T. Fernandez-Diaz, T. Ito, K. Kihou, H. Matsuhata, M. Braden, and K. Yamada, J. Phys. Soc. Jpn. **77**, 083704 (2008).
[16] A. Kreyssig, M. A. Green, Y. Lee, G. D. Samolyuk, P. Zajdel, J. W. Lynn, S. L. Bud'ko, M. S. Torikachvili, N. Ni, S. Nandi, J.

B. Leao, S. J. Poulton, D. N. Argyriou, B. N. Harmon, R. J. McQueeney, P. C. Canfield, and A. I. Goldman, Phys. Rev. B **78**, 184517 (2008).
[17] P. C. Canfield, S. L. Bud'ko, N. Ni, J. Q. Yan, A. Kracher, arXiv:0904.3134 (unpublished).
[18] A. S. Sefat, A. Huq, M. A. McGuire, R. Jin, B. C. Sales, D. Mandrus, L. M. D. Cranswick, P. W. Stephens, and K. H. Stone, Phys. Rev. B **78**, 104505 (2008).
[19] C. Wang, Y. K. Li, Z. W. Zhu, S. Jiang, X. Lin, Y. K. Luo, S. Chi, L. J. Li, Z. Ren, M. He, H. Chen, Y. T. Wang, Q. Tao, G. H. Cao, and Z. A. Xu, Phys. Rev. B **79**, 054521 (2009).
[20] G. Cao, S. Jiang, X. Lin, C. Wang, Y. Li, Q. Tao, Z. A. Xu, and F.-C. Zhang, Phys. Rev. B **79**, 174505 (2009).
[21] J.-H. Chu, J. G. Analytis, C. Kucharczyk, and I. R. Fisher, Phys. Rev. B **79**, 014506 (2009).
[22] N. Ni, M. E. Tillman, J.-Q. Yan, A. Kracher, S. T. Hannahs, S. L. Bud'ko, and P. C. Canfield, Phys. Rev. B **78**, 214515 (2008).
[23] L. J. Li, Q. B. Wang, Y. K. Luo, H. Chen, Q. Tao, Y. K. Li, X. Lin, M. He, Z. W. Zhu, G. H. Cao, and Z. A. Xu, New J. Phys. **11**, 025008 (2009).
[24] W. Schnelle, A. Leithe-Jasper, R. Gumeniuk, U. Burkhardt, D. Kasinathan, and H. Rosner, arXiv:0903.4668, Phys. Rev. B (to be published).
[25] F. Han, X. Zhu, Y. Jia, L. Fang, P. Cheng, H. Luo, B. Shen, and H. H. Wen, arXiv:0902.3957 (unpublished).
[26] X. Zhu, F. Han, P. Cheng, B. Shen, and H.-H. Wen, arXiv:0903.0323 (unpublished).
[27] G. Wu, R. H. Liu, H. Chen, Y. J. Yan, T. Wu, Y. L. Xie, J. J. Ying, X. F. Wang, D. F. Fang, and X. H. Chen, Europhys. Lett. **84**, 27010 (2008).
[28] X. F. Wang, T. Wu, G. Wu, H. Chen, Y. L. Xie, J. J. Ying, Y. J. Yan, R. H. Liu, and X. H. Chen, Phys. Rev. Lett. **102**, 117005 (2009).
[29] J.-Q. Yan, A. Kreyssig, S. Nandi, N. Ni, S. L. Bud'ko, A. Kracher, R. J. McQueeney, R. W. McCallum, T. A. Lograsso, A. I. Goldman, and P. C. Canfield, Phys. Rev. B **78**, 024516 (2008).
[30] S. R. Saha, N. P. Butch, K. Kirshenbaum, and J. Paglione, arXiv:0811.3940 (unpublished).
[31] G. Mu, H. Luo, Z. Wang, L. Shan, C. Ren, and H.-H. Wen, Phys. Rev. B **79**, 174501 (2009).
[32] R. E. Baumbach, J. J. Hamlin, L. Shu, D. A. Zocco, N. M. Crisosto, and M. B. Maple, New J. Phys. **11**, 025018 (2009).
[33] N. Kumar, R. Nagalakshmi, R. Kulkarni, P. L. Paulose, A. K. Nigam, S. K. Dhar, and A. Thamizhavel, Phys. Rev. B **79**, 012504 (2009).
[34] G. Mu, X. Zhu, L. Fang, L. Shan, C. Ren, and H. Wen, Chin. Phys. Lett. **25**, 2221 (2008).
[35] L. Ding, C. He, J. K. Dong, T. Wu, R. H. Liu, X. H. Chen, and S. Y. Li, Phys. Rev. B **77**, 180510(R) (2008).
[36] F. Han, X. Zhu, P. Cheng, B. Shen, and H. H. Wen, arXiv:0903.1028 (unpublished).
[37] I. I. Mazin, D. J. Singh, M. D. Johannes, and M. H. Du, Phys. Rev. Lett. **101**, 057003 (2008).
[38] K. Kuroki, S. Onari, R. Arita, H. Usui, Y. Tanaka, H. Kontani, and H. Aoki, Phys. Rev. Lett. **101**, 087004 (2008).
[39] F. Wang, H. Zhai, Y. Ran, A. Vishwanath, and D. H. Lee, Phys. Rev. Lett. **102**, 047005 (2009).
[40] Q. Han, Y. Chen, and Z. D. Wang, EPL **82**, 37007 (2008).
[41] D. K. Pratt, W. Tian, A. Kreyssig, J. L. Zarestky, S. Nandi, N. Ni, S. L. Bud'ko, P. C. Canfield, A. I. Goldman, and R. J. McQueeney, arXiv:0903.2833 (unpublished).
[42] E. D. Bauer, F. Ronning, B. L. Scott, and J. D. Thompson, Phys. Rev. B **78**, 172504 (2008).